



HHS Public Access

Author manuscript

Clin Cancer Res. Author manuscript; available in PMC 2020 March 15.

Published in final edited form as:

Clin Cancer Res. 2019 September 15; 25(18): 5663–5673. doi:10.1158/1078-0432.CCR-19-0366.

BAP1 loss is associated with DNA methylomic repatterning in highly aggressive Class 2 uveal melanomas

Matthew G. Field, Jeffim N. Kuznetsov, Parker L. Bussies, Louie Cai, Karam A. Alawa, Christina L. Decatur, Stefan Kurtenbach, J. William Harbour

Bascom Palmer Eye Institute, Sylvester Comprehensive Cancer Center and Interdisciplinary Stem Cell Institute, University of Miami Miller School of Medicine, Miami, FL

Abstract

Purpose: The strong association between *BAP1* mutations and metastasizing Class 2 uveal melanoma (UM) suggests that epigenetic alterations may play a significant role in tumor progression. Thus, we characterized the impact of *BAP1* loss on the DNA methylome in UM.

Experimental Design: Global DNA methylation was analyzed in 47 Class 1 and 45 Class 2 primary UMs and in UM cells engineered to inducibly deplete *BAP1*. RNA-Seq was analyzed in 80 UM samples and engineered UM cells.

Results: Hypermethylation on chromosome 3 correlated with downregulated gene expression at several loci, including 3p21 where *BAP1* is located. Gene set analysis of hypermethylated and downregulated genes identified axon guidance and melanogenesis as deregulated pathways, with several of these genes located on chromosome 3. A novel hypermethylated site within the *BAP1* locus was found in all Class 2 tumors, suggesting that *BAP1* itself is epigenetically regulated. Highly differentially methylated probes were orthogonally validated using bisulfite sequencing, and they successfully distinguished Class 1 and Class 2 tumors in 100% of cases. In functional validation experiments, *BAP1* knockdown in UM cells induced methylomic repatterning similar to UM tumors, enriched for genes involved in axon guidance, melanogenesis, and development.

Conclusions: This study, coupled with previous work, suggests that the initial event in the divergence of Class 2 UM from Class 1 UM is loss of one copy of chromosome 3, followed by mutation of *BAP1* on the remaining copy of chromosome 3, leading to the methylomic repatterning profile characteristic of Class 2 UMs.

Corresponding author: J. William Harbour, MD, 900 SW 17th Street, Miami, FL 33136, phone: (305) 326-6166, fax: (305) 326-6417, harbour@miami.edu.

Author contributions: M.G.F. helped design and conduct the experiments, analyzed and interpreted the data and wrote the manuscript. C.L.D. collected and prepared the samples, maintained the clinical database and oversaw regulatory compliance. P.B. collected, analyzed and interpreted the data and helped write the manuscript. L.C. and K.A. helped analyze the data and revise the manuscript. J.K. and S.K. helped design and conduct the experiments and analyze the data. J.W.H. secured funding, designed and led the project, provided clinical samples, interpreted the data and wrote the manuscript.

Conflicts of Interest: Dr. Harbour is an inventor of intellectual property discussed in this study. He is a paid consultant for Castle Biosciences, licensee of this intellectual property, and he receives royalties from its commercialization. All remaining authors declare no competing financial interests.

Accession codes: All methylation and RNA-Seq data generated in this study have been deposited in Gene Expression Omnibus under accession code GSE130357.

Translational Relevance: We provide evidence that bi-allelic loss of *BAP1* leads to extensive methylomic repatterning that results in the highly aggressive Class 2 phenotype, thereby providing a more complete picture of UM genomic evolution and potentially explaining the loss of melanocytic differentiation and gain of neural crest-like migratory behavior in Class 2 UM. Highly differentially methylated sites were identified that could form the basis for liquid biopsy biomarkers. These findings suggest a potential role for DNA methylation modulators in the treatment of UM.

Introduction

Uveal melanoma (UM) is the most common primary cancer of the eye, leading to fatal hematogenous metastasis in up to half of patients (1). In recent years, considerable progress has been achieved in elucidating the molecular landscape of UM (2). Primary UMs can be divided into two prognostically significant categories based on their gene expression profile (GEP), which remains the most accurate prognostic method for this cancer (3–7). UMs with the Class 1 GEP have low metastatic risk, whereas those with the Class 2 GEP have high metastatic risk. To provide a standardized instrument for classifying UMs based on GEP, a 12-gene prognostic test was developed and validated for routine clinical use in a Collaborative Ocular Oncology Group (COOG) prospective study of 459 patients (8,9). The transcriptome of Class 1 UMs corresponds to that of differentiated melanocytes and Class 2 UMs to that of neural crest-like progenitors from which uveal melanocytes arise (10,11), suggesting that aberrations may accrue during progression to Class 2 UM that disrupt the transcriptomic program maintaining cells in a differentiated melanocytic cell fate. We previously found that Class 2 UMs harbor loss-of-function mutations in *BAP1*, located on chromosome 3p21, and that the other copy of *BAP1* is lost as a result of monosomy 3 or isodisomy 3 (12), thereby fulfilling Knudson’s “two hit” hypothesis for tumor suppressors (13). The discovery of *BAP1* mutations finally explained the association between monosomy 3 and poor prognosis in UM that had been known for almost three decades with no mechanistic explanation (14). However, in contrast to other *BAP1*-associated cancers such as renal cell carcinoma and mesothelioma, where *BAP1* is frequently eliminated by regional deletions around the gene locus (15,16), Class 2 UMs demonstrate complete loss of an entire copy of chromosome 3 (14,17). Indeed, partial deletion of chromosome 3 is associated with low risk Class 1 UMs (17).

A critical unanswered question is why complete loss of chromosome 3 is required in UM for the Class 2 GEP and high metastatic risk. One possibility is that haploinsufficiency for multiple genes across the chromosome may be required for malignant progression, but this is unlikely since isodisomy 3 (loss of one copy of chromosome 3 and duplication of the remaining *BAP1* mutation-bearing copy of chromosome 3) confers the same Class 2 GEP and metastatic risk as monosomy 3 (17,18). A second possibility is that other tumor suppressor genes on chromosome 3 are also mutated in Class 2 tumors, and that these must also be reduced to homozygosity in order for the Class 2 phenotype to emerge (19). However, intensive investigations in using next generation sequencing have failed to identify any commonly mutated genes on chromosome 3 other than *BAP1* (12,17,20–22). A third possibility is that the retained copy of chromosome 3 in Class 2 tumors contains not only a mutant copy of *BAP1*, but also epigenetic alterations that are required for the Class 2

phenotype. If this model is correct, it raises the question of whether *BAP1* loss might itself contribute to this epigenetic reprogramming. Here, we used an integrated transcriptomic, methylomic and functional approach to address this question. Our findings provide evidence in support of the third model. *BAP1*-mutant Class 2 UMs exhibit extensive non-random alterations in DNA methylation, many of which are located on chromosome 3 and some of which may be specifically triggered by loss of *BAP1*. This study identifies novel prognostic biomarkers and provides functional evidence linking *BAP1* loss to specific methylomic alterations, suggesting new therapeutic strategies in *BAP1*-mutant tumors.

Materials and Methods

Patient samples and acquisition of publicly available data

This study was approved by the Institutional Review Board and adhered to the tenets of the Declaration of Helsinki. Written informed consent was obtained from each patient. Primary UM samples were obtained at enucleation, snap frozen and stored at -80°C . DNA was extracted using QIAamp DNA Mini Kit (Qiagen). DNA methylation analysis was performed on the Infinium Human Methylation 450K BeadChip Kit (Illumina, Inc.). In addition, raw data files from the 80 TCGA UM samples, which were also analyzed on the Infinium Human Methylation 450K BeadChip system (22), were obtained from the Cancer Genomics Hub (CGHub). Methylation data underwent quality control, normalization, batch identification with singular value decomposition and correction with Empirical Bayes frameworks, and analysis using the ChAMP methylation pipeline in R (23). Unsupervised principal component analysis (PCA) and 3D visualization were performed on the top 20% most variably methylated probes using the stats and rgl packages in R and ellipsoids were plotted at 95% confidence intervals. RNA-Sequencing data from TCGA was analyzed as previously described (24) and then assessed for differential expression using EdgeR (25) and DESeq2 (26). Significantly differentially expressed genes found with both EdgeR and DESeq2 were used for downstream analyses. Plots of the number of significant probe sites in CpG-island feature, chromosome, or promoter regions were normalized to the overall number of probes present within each of those regions contained in the Infinium Human Methylation 450K BeadChip Kit and statistical significance was assessed using binomial testing. Genomic locations are expressed using the hg19/GRCh37 assembly.

Integrated analysis of methylation and gene expression

Gene expression and associated methylation probe sites that were both significantly different ($\text{FDR} < 0.05$) between Class 1 and Class 2 tumors from the TCGA dataset consisting of 80 UM samples were compared using custom scripts in R. For genes with multiple significantly methylated probe sites, downstream analyses were conducted based on the average and sum of all significantly methylated probes, as well as sequential and reverse sequential numeric ordering of the Delta Beta (Class 2 Beta – Class 1 Beta) methylation values with removal of additional probe sites for each gene. Primary findings of downstream analyses using each strategy showed similar results and reverse sequential numeric ordering of the Delta Beta values with removal of additional probe sites for each gene was selected for determination of gene quadrant location. Results were plotted in a quadrant graph comparing methylation and gene expression using ggplot2 in R. Quadrants that showed significant 1) hypermethylation

and downregulated gene expression and 2) hypomethylation and upregulated gene expression were selected for subsequent analyses; further filtering included an absolute value ($\log_2(\text{RNA fold change}) > 1$ and absolute value (methylation Delta Beta value) > 0.05 . RNA fold change was defined as the Class 2 RNA normalized count divided by the Class 1 RNA normalized count with normalization conducted in DeSeq2 as described (26). Circular plots of DNA methylation from probes within those quadrants were generated using the Perl-based Circos graphical program (27). Methylation location with respect to CpG sites and expression data of specific chromosomal regions were plotted using ggpubr, ggplot2, and GViz in R (28). Predictions of transcription factor binding sites within DNA regions were conducted using PROMO (29).

Pathway analysis

Differentially hypermethylated/downregulated genes and hypomethylated/upregulated genes were input into Gene Set Enrichment Analysis (GSEA) (30), which uses hypergeometric distribution to look for significant enrichment ($\text{FDR} < 0.05$) within annotated gene sets in the Molecular Signatures Database (MSigDB), including chromosomal location, transcription factor target binding, and KEGG and Reactome functional pathway gene sets. Protein-protein interaction networks of significantly enriched functional pathway gene sets were generated using STRING (31) and modified in Adobe Illustrator (Adobe Systems Inc.).

Probe selection for orthogonal validation

For validation of selected sites that were highly differentially methylated in Class 2 tumors, we filtered by hypermethylated CpG sites ($\text{FDR} < 0.05$) that correlated with significantly downregulated gene expression ($\text{FDR} < 0.05$) in Class 2 tumors compared to Class 1. Additionally, to filter out differentially methylated sites arising from infiltrating immune cells, we obtained a publicly available dataset of 6 whole blood samples analyzed on the Infinium Human Methylation 450K BeadChip Kit (Illumina, Inc.) (32) and analyzed this dataset as described above. Class 1 and Class 2 samples were compared to the whole blood methylation data, and probes were discarded if there was hypermethylation in the whole blood cell data compared to Class 1 or Class 2 samples. Next, to control for whether chromosomal aberrations may have biased the findings, probes were selected from genes in chromosomal regions frequently gained or lost in UM tumors (chr 1, 3, 6, and 8). Further probe selection was based on identifying probes from genes within those chromosomes that showed the greatest difference in methylation between Class 2 UMs when compared to both Class 1 UMs and WBCs and/or finding genes with multiple top hit probes that could be targeted with the same primer pair. The number of probes chosen for validation was limited due to the available DNA from fresh tumor samples. The genes that were selected, their chromosomal locations, the CpG probes targeted, and the forward and reverse primers targeting the sites were designed using Zymo Bisulfite Primer Seeker (Zymo Research) for each region of interest and were optimized to ensure specificity to bisulfite-converted DNA.

Orthogonal validation of selected methylation sites and assessment of prognostic value

Genomic DNA was extracted using the Wizard Genomic DNA Purification kit (Promega) according to manufacturer instructions from 14 primary UM tumors (five Class 1 and nine Class 2). 2 μg of DNA from each sample was bisulfite converted using EZ DNA

Methylation-Lightning Kit (Zymo Research) according to manufacturer instructions and subsequently PCR amplified with the appropriate primers (Supplementary Table S1) using Epimark Hot Start Taq DNA Polymerase (New England Biolabs). PCR products were purified by agarose gel separation and extracted with the QIAquick Gel Extraction Kit (Qiagen). Sanger sequencing was conducted for each respective sample and primer site. CLC Sequence Viewer 7 (Qiagen) was used to align sequences, and SnapGene Viewer (GSL Biotech LLC) was used to visualize the sequencing traces and make methylation calls. CpG methylation probe site calls within the sequencing region of each primer pair were compiled independently by two investigators who were masked to all clinical information. In most methylation probe locations, either an unmethylated (T) or methylated (C) peak clearly predominated. At sites with ~50% methylation, the call was made as a Y (representing the co-occurrence of both methylation and non-methylation). No discordance in calls between investigators occurred. After all methylation calls were made, the results were used to predict molecular prognostic class assignments (Class 1 or Class 2), which was independently determined using a prospectively validated 15-gene expression profile prognostic test performed in a CAP-accredited, CLIA-certified laboratory (33).

Inducible BAP1 knockdown cell lines

Short hairpin RNA (shRNA) vectors targeting CGTCCGTGATTGATGATGATA, CCCTGTATATGGATTTATCTT, and CCACAACACTACGATGAGTTCAT of human *BAP1* cDNA (shBAP1) were individually cloned into a pLKO-TET-puro vector (Addgene #21915) and packaged into lentiviral particles by transient transfection into H293T cells, as previously described (34). UM cell lines Mel202 and 92.1 (kindly provided by Drs. B. Ksander and M. Jager, respectively) were then transduced with shBAP1-containing lentiviral particles and selected with puromycin (2 µg/ml) 48 h after initial transduction. Cells were clonally selected for optimal doxycycline-inducible BAP1 knockdown (>85% knockdown) and expanded for use in this study. Cells were grown to <80% confluency and induced with 1 µg/ml of doxycycline for 5 days. After 5 days of doxycycline induction, BAP1 knockdown (BAP1KD) was confirmed by western blot using an anti-BAP1 primary antibody (Santa Cruz, H-300), anti-β-actin loading control antibody (Cell Signaling Technology, 4967S), IRDye and VRDye secondary antibodies (Li-COR Biosciences), and a LI-COR Odyssey CLx imaging system. Genomic DNA was isolated using QIAamp DNA Mini Kit (Qiagen) and RNA was isolated using TriZol and the RNeasy Mini RNA isolation kit with RNAase-Free DNase treatment (Qiagen). Uninduced cells were used as a control.

Global methylation and RNA analysis of BAP1 knockdown cells

Genomic DNA from control and doxycycline-induced BAP1KD Mel202 and 92.1 UM cells were analyzed using the Infinium Methylation EPIC BeadChip Kit (Illumina, Inc.), with two biological replicates for each condition. Methylation data underwent quality control, normalization, batch correction, and analysis using the ChAMP methylation pipeline in R (23). Significantly hypermethylated or hypomethylated probes (FDR < 0.05) were identified with cell lines pooled together when comparing BAP1KD to control cells. RNA-seq libraries were prepared using the TruSeq Stranded Total RNA prep kit with Ribo-Zero Gold to remove cytoplasmic and mitochondrial rRNA according to the manufacturer's recommendation (Illumina, Inc.). Total RNA-seq libraries were ran on an Illumina NextSeq

500 sequencing instrument according to the protocols described by the manufacturer (Illumina, Inc.). Raw RNA-Seq FASTQ files were assessed for quality using FastQC and aligned to the genome with count files generated using STAR (35). Read counts were normalized and batch corrected then assessed for differences in expression ($p < 0.05$) between groups using EdgeR (25). After library prep and quality control, two biological replicates were obtained for each condition from 92.1 cells and one each for Mel202 cells and the data was pooled together. Similar to the TCGA data analysis, hypermethylated/downregulated and hypomethylated/upregulated genes ($p < 0.05$) were selected for subsequent analyses; further filtering included an absolute value ($\log_2(\text{RNA fold change}) > 1$ and absolute value (methylation Delta Beta value) > 0.01). RNA fold change was defined as the doxycycline-induced BAP1KD RNA normalized count divided by the un-induced RNA normalized count. Genes with significant hypermethylation/downregulation or hypomethylation/upregulation from the BAP1KD cells ($p < 0.05$) were compared with hypermethylated/downregulated and hypomethylated/upregulated genes from the TCGA dataset ($FDR < 0.05$). Overlap of individual probes between datasets was also assessed. Chromosomal location and pathway analyses were conducted using GSEA and MSigDB as described above.

Results

Global DNA methylation profiling

Primary UMs can be divided based on DNA methylomic profiling into two groups that correspond to *BAP1* mutation status and clinical GEP classification (Class 1 versus Class 2) (17,22). To elucidate methylation changes associated with *BAP1* mutations, we performed unsupervised principal component analysis (PCA) of the top 20% most differentially methylated probes on two datasets, including the 80 TCGA samples and 12 independent samples from our center, both analyzed on the Infinium Human Methylation 450K BeadChip array (Supplementary Table S2). As expected, tumor samples from both datasets clustered into two distinct groups corresponding to Class 1/*BAP1*-wildtype and Class 2/*BAP1*-mutant subtypes (Fig. 1A–B). Of the 20% most variable probes, 82% were shared between datasets, and out of the top 5000 probes making the greatest contribution to the first principal component (PC1), 204 probes were shared between datasets (Supplementary Table S2). Next, we sought to obtain functional insights into the methylation changes. Hypermethylated probes in Class 2 UMs relative to Class 1 UMs ($FDR < 0.05$) were most enriched within “shore” regions 1000–1500 bp upstream of transcription start sites (TSS-1500), followed by “shore” regions in the 5'UTR and “shelf” regions within the TSS-1500 (Fig. 1C, Supplementary Table S2). Notably, methylation in these “shore” regions correlated inversely with gene expression (36). Hypomethylated probes in Class 2 UMs relative to Class 1 UMs ($FDR < 0.05$) were most enriched in open sea regions. Hyper- and hypomethylated probes ($FDR < 0.05$) within promoter regions were significantly enriched on chromosomes 3 and 8 (Fig. 1D), which commonly display copy number alterations in UM (17). In particular, chromosome 3, which is reduced to homozygosity in most Class 2 tumors, demonstrated the most significant enrichment for promoter hypermethylation in Class 2 tumors (Fig. 1D). These findings suggest that the sole copy of chromosome 3 in

Class 2/*BAP1*-mutant UM harbors extensive epigenetic alterations that may play a role in tumor progression.

Integrated analysis of DNA methylation and RNA expression

To further explore the potential functional relevance of these findings, we then focused on integrating methylation with gene expression. As hypermethylation in promoter regions is usually associated with gene silencing (37), we identified genes with hypermethylation associated with decreased gene expression (hypermethylated/downregulated) or hypomethylation associated with increased gene expression (hypomethylated/upregulated) in Class 2 UMs relative to Class 1 UMs (Fig. 2A). This analysis revealed 1621 hypermethylated probes associated with 508 downregulated genes (FDR < 0.05) and 3876 hypomethylated probes associated with 923 upregulated genes (FDR < 0.05) (Supplementary Table S3). Out of the twelve genes in the GEP test, six of the eight downregulated genes were hypermethylated (*FXR1*, *ID2*, *ROBO1*, *LMCD1*, *SATB1*, and *MTUS1*) and all four of the upregulated genes were hypomethylated (*HTR2B*, *ECM1*, *RAB31*, *CDH1*). Similar to our global analysis, hypermethylated/downregulated genes in Class 2 tumors were enriched within the promoter and 5'UTR "shore" and "shelf" regions (Fig. 2B), and hypomethylated/upregulated genes in Class 2 tumors occurred mostly in open sea regions (38). Chromosomal regions that were significantly enriched (FDR < 0.05) for hypermethylated/downregulated genes included 6p21, 6p24, 19q13, 10q24, 4p14, as well as multiple regions on chromosome 3 (3p21–23, 3p25–26, 3q12–21, and 3q27). Regions enriched (FDR < 0.05) for hypomethylated/upregulated genes included 6p21, 17q21, 15q21, and 12p13, 22q13, 1q31, and several regions on chromosome 8 (8p21, 8q13, 8q21–22)(Fig. 2A–C and Supplementary Table S4). Interestingly, 6p21 contains regions of both hypomethylated/upregulated and hypermethylated/downregulated genes in Class 2 tumors, but only the former is enriched for HLA genes, which are known to be expressed as part of the altered immune microenvironment in Class 2 tumors.

Functional pathway analysis

Both hypermethylated/downregulated and hypomethylated/upregulated regions were enriched for genes with functions related to developmental biology and tissue development, focal adhesion, immune function and axon guidance (Supplementary Table S4), and they were enriched for regulatory binding sites for the transcription factors TCF3, TFAP4, FOXO4 and LEF1 (Supplementary Table S4), which are associated with cell fate, differentiation, stem cell maintenance, tumor growth, and metastasis (39,40). Of note, LEF1 and TCF3 are important for melanocyte lineage commitment through their interaction with the *MITF* promoter, and they are involved in WNT signaling and axon guidance (41,42). Since melanogenesis was one of the top pathways for hypermethylated/downregulated genes, we inspected *MITF*, which did not meet our strict RNA-Seq logFC cutoff, although it did exhibit significant hypermethylation and decreased gene expression (FDR < 0.05 for both) in Class 2 UMs relative Class 1 UMs. Furthermore, axon guidance was one of the most significant pathways for both hypermethylated/downregulated and hypomethylated/upregulated genes, many of which are involved in migration of neural crest from which melanocytes arise (Fig. 3)(43–45). The proteins encoded by these axon guidance and melanogenesis genes demonstrated extensive interactome connectivity (Fig. 3) and share

many of the same transcription factor binding sites, suggesting that they may be de-regulated in a functionally significant manner.

Epigenetic alterations on chromosome 3

Plotting all hypermethylated/downregulated and hypomethylated/upregulated probes along the length of chromosome 3 demonstrates the extensive hypermethylation/downregulation occurring in Class 2 UM, with the most significant probes and highest methylation fold changes occurring within the previously identified chromosomal loci (3p26–25, 3p23–21, 3q12–21, and 3q27) that are enriched (FDR < 0.05) in hypermethylated/downregulated genes (Fig. 4). Of particular interest, these regions on chromosome 3 contained many of the axon guidance and melanogenesis genes described above, including *DVL3*, *RAF1*, *MITF*, *SATB1*, *PLXNB1*, *CHL1*, *ROBO1*, and *SEMA3B* (Fig. 4). Hypermethylated probes were present in the promoter region of all of these genes with the exception of *ROBO1*, which had several hypermethylated sites located within the gene body. Several of these genes (*MITF*, *ROBO1*, and *SEMA3B*) had both hypermethylated and hypomethylated sites distributed throughout gene body exons, suggesting that epigenetic regulation of these genes is complex and may involve splicing, alternative exon usage, or other regulatory mechanisms. Consistent with previous work (12,46), no significant differences in methylation of the *BAP1* promoter region were found between Class 2 and Class 1 UMs or between monosomy 3 and disomy 3 UMs. Interestingly, however, *BAP1* is located within one of the hypermethylated/downregulated loci on chromosome 3 (3p21) and contained two significantly hypermethylated CpG probe sites (FDR < 0.05), one of which was located within the gene body (cg16871520) and the other in the 3'UTR (cg21746711)(Fig. 5). The cg16871520 probe demonstrated the most significant inverse Spearman correlation coefficient between *BAP1* gene expression and methylation ($R=-0.79$, $p < 0.001$). This single probe accurately distinguished Class 1 UMs from Class 2 UMs in 79 out of the 80 samples (Fig. 5).

Orthogonal validation of methylated loci

Several of the most significantly hypermethylated probes from the hypermethylated/downregulated genes in Class 2 UMs were selected for orthogonal validation using the bisulfite conversion method, including *IL12RB2* (chr1, 6 probes), *SATB1* (chr3, 1 probe), *SESNI* (chr6, 1 probe), and *ENPP2* (chr8, 2 probes)(Supplementary Table S1). CpG methylation was assessed for sites within the sequencing region of each primer pair in an independent dataset of 14 primary UM samples (distinct from the 12 independent UM samples used for methylation array analysis), including five Class 1 and nine Class 2 tumors. Class 1 tumors were readily distinguished from the Class 2 tumors by the methylation status of these probes (Fig. 6). The probes that most accurately differentiated Class 1 UMs from Class 2 UMs were the *IL12RB2* probes and the *SESNI* probe.

Functional validation of methylation and gene expression changes attributable to *BAP1* loss

To determine if methylomic repatterning in Class 2 UM is directly attributable, at least in part, to *BAP1* loss, we engineered UM cell lines Mel202 and 92.1 to allow efficient BAP1KD using a Tet-inducible shBAP1 system (Supplementary Fig. S1A). Following

BAP1KD, the BAP1KD 92.1 and Mel202 cells clustered together and away from their respective control cells (Supplementary Fig. S1B-C) with 11,023 hypermethylated and 3,864 hypomethylated probes (FDR < 0.05) occurring within 4,481 and 2,153 genes, respectively (Supplementary Table S5). Consistent with findings in Class 2 UMs, development, axon guidance, and melanogenesis pathways were significantly enriched (FDR < 0.05) for genes with hypermethylated probes (FDR < 0.05) in the BAP1KD UM cell lines, which also showed the most significant hypermethylated loci enrichment for chromosomal band 3p21, where *BAP1* is located, as well as another locus on chromosome 3 at 3q21 (FDR < 0.05, Supplementary Table S5). Similarly to the Class 2 UMs, immune function, focal adhesion, and axon guidance pathways were significantly enriched for hypomethylated genes (FDR < 0.05).

After integrating methylation data with matched RNA-Seq data, there were 417 significantly hypermethylated/downregulated genes and 110 hypomethylated/upregulated genes ($p < 0.05$) in the BAP1KD cells (Supplementary Table S6). Again, development, axon guidance, and melanogenesis were among the pathways most significantly enriched for hypermethylated/downregulated genes in BAP1KD UM cell lines (FDR < 0.05), whereas loci on chromosome 3 were no longer significantly enriched (Supplementary Table S6). Hypomethylated/upregulated genes from the BAP1KD cells were significantly enriched for pathways involved in apoptosis and cell death (FDR < 0.05). Of the 12 genes from the GEP test, *ROBO1* and *MTUS1* became hypermethylated after BAP1KD, but none of the genes showed corresponding changes in methylation and gene expression.

Next, we compared BAP1KD cells to Class 2 UMs from the TCGA dataset, and we found 31 hypermethylated/downregulated and 9 hypomethylated/upregulated genes shared in common. Four of the 31 genes were in the development (*ACVR2B*, *ADCY6*, *DPYSL2*, *ROBO3*), two in the axon guidance (*DPYSL2*, *ROBO3*) and one in the melanogenesis (*ADCY6*) pathway. For individual probes, only two exact probe sites (one on *PC* and one on *PALMD*) were shared for the hypermethylated/downregulated genes and one (*ZEB1*) for the hypomethylated/upregulated genes. Interestingly, a recent paper has correlated *ZEB1* upregulation with metastatic progression of UM, showing functionally that *ZEB1* promotes UM dedifferentiation, depigmentation, and increased invasiveness (47). Overall, these findings confirm that loss of *BAP1* leads to DNA methylomic repatterning, as recently described in liver cancer (48), with the most extensive changes in UM occurring in the axon guidance and melanogenesis pathways.

Discussion

Here, we found that Class 2/*BAP1* mutant UMs share a common DNA methylation profile reflecting extensive methylomic repatterning compared to Class 1/*BAP1* wildtype UMs. The stereotyped nature of the methylomic profile and its strong association with *BAP1* loss suggest that it may represent a latent epigenetic program regulated by *BAP1* within the melanocyte/neural crest lineage. Consistent with this possibility, melanogenesis was one of the most significantly enriched functional pathways among hypermethylated/downregulated genes in Class 2 UMs, a finding concordant with the impairment of melanocyte differentiation in this subclass. Among the downregulated melanogenesis genes, *EDNRB*

mediates commitment of neural crest cells to the melanocyte lineage, *MITF* is the master regulator of melanocyte differentiation, and *DCT* is an enzyme in the melanin synthesis pathway and is one of the earliest markers specific to melanocyte differentiation (49–51). Additionally, the axon guidance pathway was a top hit for both hypermethylated/downregulated and hypomethylated/upregulated genes, demonstrating an extensive protein-protein interactome between all members (Fig. 3). This connectivity, even among inversely correlated genes, is a manifestation of the complex interaction of both attractive and repulsive cues coordinating migration and differentiation in the neural crest lineage. For example, the hypermethylated/downregulated axon guidance genes *ROBO1*, *PLXNB1*, *SEMA3B*, and *CHL1* are involved in neuronal/neural crest migration but have been implicated as tumor suppressors (45,52–54), whereas the hypomethylated/upregulated *SEMA3E* is an axonal path finding gene that increases tumor invasiveness and metastatic spread (55). These findings are consistent with recent work showing that *BAP1* regulates neural crest migration and melanogenesis during vertebrate development (Dawn Owens, PhD, personal communication) and could explain why Class 1/*BAP1*-wildtype UMs demonstrate characteristics of differentiated melanocytes, whereas Class 2/*BAP1*-mutant UMs resemble neural crest-like progenitor cells (10,11).

Additionally, the most significant and densely clustered hypermethylated/downregulated gene loci in Class 2 UMs were located on chromosome 3, which contained many of the axon guidance cue, neural crest specification, and melanocyte differentiation genes (e.g., *ROBO1*, *PLXNB1*, *SEMA3B*, *CHL1*, *SATB1*, *MITF*, *DVL3*, and *RAF1*). Since all of these genes undergo repressive methylation changes on the sole remaining copy of chromosome 3, this could explain why the other copy of chromosome 3 must be lost in order to acquire the metastasizing Class 2 UM phenotype, as has been hypothesized previously (56,57). The cg16871520 probe, which detects methylation in the *BAP1* gene body, demonstrated a highly significant association between increased methylation and Class 2 GEP. As such, methylation sites in this region could potentially represent valuable new biomarkers. Since all but three Class 2 tumors in this analysis had detectable inactivating *BAP1* mutations, it is not clear how hypermethylation of the gene would be functionally relevant to conversion to Class 2. *BAP1* may negatively regulate its own methylation, as it does with the neural crest and melanogenesis genes described above, such that loss of *BAP1* could lead to hypermethylation of the remaining allele as a “passenger event” in the absence of selective pressure, though this was not seen in the *BAP1*KD cells. Furthermore, experimental *BAP1*KD did show an enrichment for hypermethylation of axon guidance and melanogenesis genes, and recapitulated hypermethylation of specific loci on chromosome 3, including 3p21 where *BAP1* is located, as observed in primary UM tumor samples. This is consistent with a recent large study that identified *BAP1* as one of several genes in which mutations were associated with global methylomic alterations (48). When pairing methylation and RNA-Seq datasets, the hypermethylated/downregulated genes in the *BAP1*KD cells maintained enrichment for axon guidance and melanogenesis pathways, however, enrichment for loci on chromosome 3 was not maintained. In terms of the GEP, ten of the twelve genes showed corresponding methylation and gene expression changes in the TCGA dataset, implicating methylation in regulating their gene expression, but this was not re-capitulated in the *BAP1*KD cells.

Of note, we would not expect the depletion of *BAP1* in 92.1 or Mel202 cells to precisely recapitulate the methylation or GEP findings in actual human Class 2 UMs. First, it is well known that cultured cells do not exactly match the tumors they were derived from. Second, the 92.1 and Mel202 cells are heterozygous for chromosome 3 and have different genetic profiles than Class 2 UMs. Accordingly, others have suggested that different populations of normal uveal melanocyte precursor cells exist in the eye with differing methylation profiles and that the specific methylation profile present may make those cells more susceptible to development of a specific UM subtype (56). Finally, knocking down *BAP1* is not equivalent to knocking down expression of the entire chromosome 3, which occurs in Class 2 UMs and is required for the Class 2 GEP. Thus, we would anticipate that the differentially methylated probes shared between the *BAP1*KD and primary UM samples would be enriched for those specifically related to *BAP1* loss but not necessarily for those related to chromosome 3 loss, tumor microenvironmental influences and other factors. Consequently, and keeping in mind the well-known differences between tumors and derivative cell lines, we would not expect an exact match of probes between these sources. Nevertheless, it is remarkable that axon guidance and melanogenesis are enriched pathways associated with *BAP1* loss in both tumor samples and cell lines, and that some of the same genes overlap between systems (i.e. *ADCY6*, *ROBO3*, *DPYSL2*). Therefore, taken in context with previous work showing the evolution of genomic aberrations in UM (17,22), we hypothesize that the initial event presaging the divergence of Class 2 UM from Class 1 UM is loss of one copy of chromosome 3, which is followed by mutation of *BAP1* on the other copy of chromosome 3, which then leads to the methylomic repatterning characteristic of Class 2 UMs. Future studies profiling the methylome of normal uveal melanocytes may provide insights into how preexisting epigenetic states may drive malignant transformation along the observed evolutionary trajectories.

Finally, we confirmed that methylation probes from the *IL12RB2*, *SATB1* and *SESNI* genes accurately differentiated Class 1 from Class 2 UMs as an orthogonal validation and as a proof-of-concept for developing a methylDNA-based liquid biopsy assay in the future. For this purpose, we filtered the probe list for hypermethylated sites found in whole blood samples in order to eliminate potential contamination from circulating immune cells. While our findings suggest that such an approach is possible and could reduce the need for invasive biopsies, several technical challenges need to be overcome that are beyond the scope of the current study.

Supplementary Material

Refer to Web version on PubMed Central for supplementary material.

Acknowledgements:

This work was supported by National Cancer Institute grants R01 CA125970 (JW Harbour) and F30 CA206430 (MG Field), Alcon Research Institute (JW Harbour), Research to Prevent Blindness, Inc. Senior Scientific Investigator Award (JW Harbour), the University of Miami Sheila and David Fuente Graduate Program in Cancer Biology (MG Field), the Center for Computational Science Fellowship (MG Field), and a generous gift from Dr. Mark J. Daily (JW Harbour). The Bascom Palmer Eye Institute also received funding from NIH Core Grant P30EY014801 and a Research to Prevent Blindness Unrestricted Grant. We are grateful to the patients who generously contributed samples for this research. We acknowledge the support of the Biostatistics & Bioinformatics

and Oncogenomics Shared Resources at the Sylvester Comprehensive Cancer Center, and the University of Miami Center for Computational Science.

References

1. Ramaiya KJ, Harbour JW. Current management of uveal melanoma. *Expert Review of Ophthalmology* 2007;2(6):939–46 doi doi:10.1586/17469899.2.6.939.
2. Harbour JW, Chao DL. A molecular revolution in uveal melanoma: implications for patient care and targeted therapy. *Ophthalmology* 2014;121(6):1281–8 doi 10.1016/j.ophtha.2013.12.014. [PubMed: 24480708]
3. Onken MD, Worley LA, Ehlers JP, Harbour JW. Gene expression profiling in uveal melanoma reveals two molecular classes and predicts metastatic death. *Cancer Res* 2004;64:7205–9. [PubMed: 15492234]
4. Tschentscher F, Husing J, Holter T, Kruse E, Dresen IG, Jockel KH, et al. Tumor classification based on gene expression profiling shows that uveal melanomas with and without monosomy 3 represent two distinct entities. *Cancer Res* 2003;63(10):2578–84. [PubMed: 12750282]
5. van Gils W, Lodder EM, Mensink HW, Kilic E, Naus NC, Bruggenwirth HT, et al. Gene expression profiling in uveal melanoma: two regions on 3p related to prognosis. *Invest Ophthalmol Vis Sci* 2008;49(10):4254–62. [PubMed: 18552379]
6. Petrusch U, Martus P, Tonnie H, Bechrakis NE, Lenze D, Wansel S, et al. Significance of gene expression analysis in uveal melanoma in comparison to standard risk factors for risk assessment of subsequent metastases. *Eye* 2007;22(8):997–1007. [PubMed: 17384575]
7. Singh AD, Sisley K, Xu Y, Li J, Faber P, Plummer SJ, et al. Reduced expression of autotaxin predicts survival in uveal melanoma. *Br J Ophthalmol* 2007;91(10):1385–92 doi 10.1136/bjo.2007.116947. [PubMed: 17475713]
8. Onken MD, Worley LA, Tuscan MD, Harbour JW. An accurate, clinically feasible multi-gene expression assay for predicting metastasis in uveal melanoma. *J Mol Diagn* 2010;12(4):461–8 doi 10.2353/jmoldx.2010.090220. [PubMed: 20413675]
9. Onken MD, Worley LA, Char DH, Augsburg JJ, Correa ZM, Nudleman E, et al. Collaborative Ocular Oncology Group report number 1: prospective validation of a multi-gene prognostic assay in uveal melanoma. *Ophthalmology* 2012;119(8):1596–603 doi 10.1016/j.ophtha.2012.02.017. [PubMed: 22521086]
10. Onken MD, Ehlers JP, Worley LA, Makita J, Yokota Y, Harbour JW. Functional gene expression analysis uncovers phenotypic switch in aggressive uveal melanomas. *Cancer Res* 2006;66(9):4602–9. [PubMed: 16651410]
11. Chang SH, Worley LA, Onken MD, Harbour JW. Prognostic biomarkers in uveal melanoma: evidence for a stem cell-like phenotype associated with metastasis. *Melanoma Res* 2008;18(3):191–200. [PubMed: 18477893]
12. Harbour JW, Onken MD, Roberson ED, Duan S, Cao L, Worley LA, et al. Frequent mutation of BAP1 in metastasizing uveal melanomas. *Science* 2010;330(6009):1410–3 doi 10.1126/science.1194472. [PubMed: 21051595]
13. Knudson AG Jr. Mutation and cancer: statistical study of retinoblastoma. *Proc Natl Acad Sci U S A* 1971;68(4):820–3. [PubMed: 5279523]
14. Prescher G, Bornfeld N, Hirche H, Horsthemke B, Jockel KH, Becher R. Prognostic implications of monosomy 3 in uveal melanoma. *Lancet* 1996;347(9010):1222–5. [PubMed: 8622452]
15. Pena-Llopis S, Vega-Rubin-de-Celis S, Liao A, Leng N, Pavia-Jimenez A, Wang S, et al. BAP1 loss defines a new class of renal cell carcinoma. *Nat Genet* 2012;e-pub ahead of print 10 June 2012; doi: 10.1038/ng.2323 doi 10.1038/ng.2323.
16. Bott M, Brevet M, Taylor BS, Shimizu S, Ito T, Wang L, et al. The nuclear deubiquitinase BAP1 is commonly inactivated by somatic mutations and 3p21.1 losses in malignant pleural mesothelioma. *Nat Genet* 2011;43:668–72 doi 10.1038/ng.855. [PubMed: 21642991]
17. Field MG, Durante MA, Anbunathan H, Cai LZ, Decatur CL, Bowcock AM, et al. Punctuated evolution of canonical genomic aberrations in uveal melanoma. *Nat Commun* 2018;9(1):116 doi 10.1038/s41467-017-02428-w. [PubMed: 29317634]

18. Worley LA, Onken MD, Person E, Robirds D, Branson J, Char DH, et al. Transcriptomic versus chromosomal prognostic markers and clinical outcome in uveal melanoma. *Clin Cancer Res* 2007;13(5):1466–71 doi 10.1158/1078-0432.CCR-06-2401. [PubMed: 17332290]
19. Cross NA, Ganesh A, Parpia M, Murray AK, Rennie IG, Sisley K. Multiple locations on chromosome 3 are the targets of specific deletions in uveal melanoma. *Eye* 2006;20(4):476–81. [PubMed: 15920570]
20. Martin M, Masshofer L, Temming P, Rahmann S, Metz C, Bornfeld N, et al. Exome sequencing identifies recurrent somatic mutations in EIF1AX and SF3B1 in uveal melanoma with disomy 3. *Nat Genet* 2013;45:933–6 doi 10.1038/ng.2674. [PubMed: 23793026]
21. Johansson P, Aoude LG, Wadt K, Glasson WJ, Warriar SK, Hewitt AW, et al. Deep sequencing of uveal melanoma identifies a recurrent mutation in PLCB4. *Oncotarget* 2015 doi 10.18632/oncotarget.6614.
22. Robertson AG, Shih J, Yau C, Gibb EA, Oba J, Mungall KL, et al. Integrative Analysis Identifies Four Molecular and Clinical Subsets in Uveal Melanoma. *Cancer Cell* 2017;32(2):204–20e15 doi 10.1016/j.ccell.2017.07.003. [PubMed: 28810145]
23. Morris TJ, Butcher LM, Feber A, Teschendorff AE, Chakravarthy AR, Wojdacz TK, et al. ChAMP: 450k Chip Analysis Methylation Pipeline. *Bioinformatics* 2014;30(3):428–30 doi 10.1093/bioinformatics/btt684. [PubMed: 24336642]
24. Field MG, Durante MA, Decatur CL, Tarlan B, Oelschlager KM, Stone JF, et al. Epigenetic reprogramming and aberrant expression of PRAME are associated with increased metastatic risk in Class 1 and Class 2 uveal melanomas. *Oncotarget* 2016 doi 10.18632/oncotarget.10962.
25. Robinson MD, McCarthy DJ, Smyth GK. edgeR: a Bioconductor package for differential expression analysis of digital gene expression data. *Bioinformatics* 2010;26(1):139–40 doi 10.1093/bioinformatics/btp616. [PubMed: 19910308]
26. Anders S, McCarthy DJ, Chen Y, Okoniewski M, Smyth GK, Huber W, et al. Count-based differential expression analysis of RNA sequencing data using R and Bioconductor. *Nat Protoc* 2013;8(9):1765–86 doi 10.1038/nprot.2013.099. [PubMed: 23975260]
27. Krzywinski M, Schein J, Birol I, Connors J, Gascoyne R, Horsman D, et al. Circos: an information aesthetic for comparative genomics. *Genome Res* 2009;19(9):1639–45 doi 10.1101/gr.092759.109. [PubMed: 19541911]
28. Helaers R, Bareke E, De Meulder B, Pierre M, Depiereux S, Habra N, et al. gViz, a novel tool for the visualization of co-expression networks. *BMC Res Notes* 2011;4:452 doi 10.1186/1756-0500-4-452. [PubMed: 22032859]
29. Farre D, Roset R, Huerta M, Adsuara JE, Rosello L, Alba MM, et al. Identification of patterns in biological sequences at the ALGGEN server: PROMO and MALGEN. *Nucleic Acids Res* 2003;31(13):3651–3. [PubMed: 12824386]
30. Subramanian A, Tamayo P, Mootha VK, Mukherjee S, Ebert BL, Gillette MA, et al. Gene set enrichment analysis: a knowledge-based approach for interpreting genome-wide expression profiles. *Proc Natl Acad Sci U S A* 2005;102(43):15545–50. [PubMed: 16199517]
31. Szklarczyk D, Morris JH, Cook H, Kuhn M, Wyder S, Simonovic M, et al. The STRING database in 2017: quality-controlled protein-protein association networks, made broadly accessible. *Nucleic Acids Res* 2017;45(D1):D362–D8 doi 10.1093/nar/gkw937. [PubMed: 27924014]
32. Reinius LE, Acevedo N, Joerink M, Pershagen G, Dahlen SE, Greco D, et al. Differential DNA methylation in purified human blood cells: implications for cell lineage and studies on disease susceptibility. *PLoS One* 2012;7(7):e41361 doi 10.1371/journal.pone.0041361. [PubMed: 22848472]
33. Harbour JW. A prognostic test to predict the risk of metastasis in uveal melanoma based on a 15-gene expression profile. *Methods Mol Biol* 2014;1102:427–40 doi 10.1007/978-1-62703-727-3_22. [PubMed: 24258991]
34. Stewart SA, Dykxhoorn DM, Palliser D, Mizuno H, Yu EY, An DS, et al. Lentivirus-delivered stable gene silencing by RNAi in primary cells. *Rna* 2003;9(4):493–501. [PubMed: 12649500]
35. Dobin A, Davis CA, Schlesinger F, Drenkow J, Zaleski C, Jha S, et al. STAR: ultrafast universal RNA-seq aligner. *Bioinformatics* 2013;29(1):15–21 doi 10.1093/bioinformatics/bts635. [PubMed: 23104886]

36. Irizarry RA, Ladd-Acosta C, Wen B, Wu Z, Montano C, Onyango P, et al. The human colon cancer methylome shows similar hypo- and hypermethylation at conserved tissue-specific CpG island shores. *Nat Genet* 2009;41(2):178–86 doi 10.1038/ng.298. [PubMed: 19151715]
37. Jones PA, Baylin SB. The epigenomics of cancer. *Cell* 2007;128(4):683–92 doi 10.1016/j.cell.2007.01.029. [PubMed: 17320506]
38. Sandoval J, Heyn H, Moran S, Serra-Musach J, Pujana MA, Bibikova M, et al. Validation of a DNA methylation microarray for 450,000 CpG sites in the human genome. *Epigenetics* 2014;6(6):692–702 doi 10.4161/epi.6.6.16196.
39. Merrill BJ, Gat U, DasGupta R, Fuchs E. Tcf3 and Lef1 regulate lineage differentiation of multipotent stem cells in skin. *Genes Dev* 2001;15(13):1688–705 doi 10.1101/gad.891401. [PubMed: 11445543]
40. Jung P, Menssen A, Mayr D, Hermeking H. AP4 encodes a c-MYC-inducible repressor of p21. *Proc Natl Acad Sci U S A* 2008;105(39):15046–51 doi 10.1073/pnas.0801773105. [PubMed: 18818310]
41. Goding CR. Mitf from neural crest to melanoma: signal transduction and transcription in the melanocyte lineage. *Genes Dev* 2000;14(14):1712–28. [PubMed: 10898786]
42. Salinas PC. Wnt signaling in the vertebrate central nervous system: from axon guidance to synaptic function. *Cold Spring Harb Perspect Biol* 2012;4(2) doi 10.1101/cshperspect.a008003.
43. York JR, Yuan T, Lakiza O, McCauley DW. An ancestral role for Semaphorin3F-Neuropilin signaling in patterning neural crest within the new vertebrate head. *Development* 2018;145(14) doi 10.1242/dev.164780.
44. Martinez D, Zuhdi N, Reyes M, Ortega B, Giovannone D, Lee VM, et al. Screen for Slit/Robo signaling in trunk neural cells reveals new players. *Gene Expr Patterns* 2018;28:22–33 doi 10.1016/j.gexp.2018.01.002. [PubMed: 29427758]
45. Li Y, Zhang XT, Wang XY, Wang G, Chuai M, Munsterberg A, et al. Robo signaling regulates the production of cranial neural crest cells. *Exp Cell Res* 2017;361(1):73–84 doi 10.1016/j.yexcr.2017.10.002. [PubMed: 28987541]
46. van de Nes JA, Nelles J, Kreis S, Metz CH, Hager T, Lohmann DR, et al. Comparing the Prognostic Value of BAP1 Mutation Pattern, Chromosome 3 Status, and BAP1 Immunohistochemistry in Uveal Melanoma. *Am J Surg Pathol* 2016;40(6):796–805 doi 10.1097/PAS.0000000000000645. [PubMed: 27015033]
47. Chen Y, Lu X, Montoya-Durango DE, Liu YH, Dean KC, Darling DS, et al. ZEB1 Regulates Multiple Oncogenic Components Involved in Uveal Melanoma Progression. *Sci Rep* 2017;7(1):45 doi 10.1038/s41598-017-00079-x. [PubMed: 28246385]
48. Woo HG, Choi JH, Yoon S, Jee BA, Cho EJ, Lee JH, et al. Integrative analysis of genomic and epigenomic regulation of the transcriptome in liver cancer. *Nat Commun* 2017;8(1):839 doi 10.1038/s41467-017-00991-w. [PubMed: 29018224]
49. Lee HO, Levorse JM, Shin MK. The endothelin receptor-B is required for the migration of neural crest-derived melanocyte and enteric neuron precursors. *Dev Biol* 2003;259(1):162–75. [PubMed: 12812796]
50. Widlund HR, Fisher DE. Microphthalmia-associated transcription factor: a critical regulator of pigment cell development and survival. *Oncogene* 2003;22(20):3035–41. [PubMed: 12789278]
51. Kawakami A, Fisher DE. The master role of microphthalmia-associated transcription factor in melanocyte and melanoma biology. *Lab Invest* 2017 doi 10.1038/labinvest.2017.9.
52. Soong J, Chen Y, Shustef EM, Scott GA. Sema4D, the ligand for Plexin B1, suppresses c-Met activation and migration and promotes melanocyte survival and growth. *J Invest Dermatol* 2012;132(4):1230–8 doi 10.1038/jid.2011.414. [PubMed: 22189792]
53. Argast GM, Croy CH, Coutts KL, Zhang Z, Litman E, Chan DC, et al. Plexin B1 is repressed by oncogenic B-Raf signaling and functions as a tumor suppressor in melanoma cells. *Oncogene* 2009;28(30):2697–709 doi 10.1038/onc.2009.133. [PubMed: 19483722]
54. Schmid RS, Maness PF. L1 and NCAM adhesion molecules as signaling coreceptors in neuronal migration and process outgrowth. *Current opinion in neurobiology* 2008;18(3):245–50 doi 10.1016/j.conb.2008.07.015. [PubMed: 18760361]

55. Casazza A, Finisguerra V, Capparuccia L, Camperi A, Swiercz JM, Rizzolio S, et al. Sema3E-Plexin D1 signaling drives human cancer cell invasiveness and metastatic spreading in mice. *J Clin Invest* 2010;120(8):2684–98 doi 10.1172/JCI42118. [PubMed: 20664171]
56. Neumann LC, Weinhausel A, Thomas S, Horsthemke B, Lohmann DR, Zeschnigk M. EFS shows biallelic methylation in uveal melanoma with poor prognosis as well as tissue-specific methylation. *BMC Cancer* 2011;11:380 doi 10.1186/1471-2407-11-380. [PubMed: 21871071]
57. Zeschnigk M, Tschentscher F, Lich C, Brandt B, Horsthemke B, Lohmann DR. Methylation Analysis of Several Tumour Suppressor Genes Shows a Low Frequency of Methylation of CDKN2A and RARB in Uveal Melanomas. *Comp Funct Genomics* 2003;4(3):329–36 doi 10.1002/cfg.295 [doi]. [PubMed: 18629284]

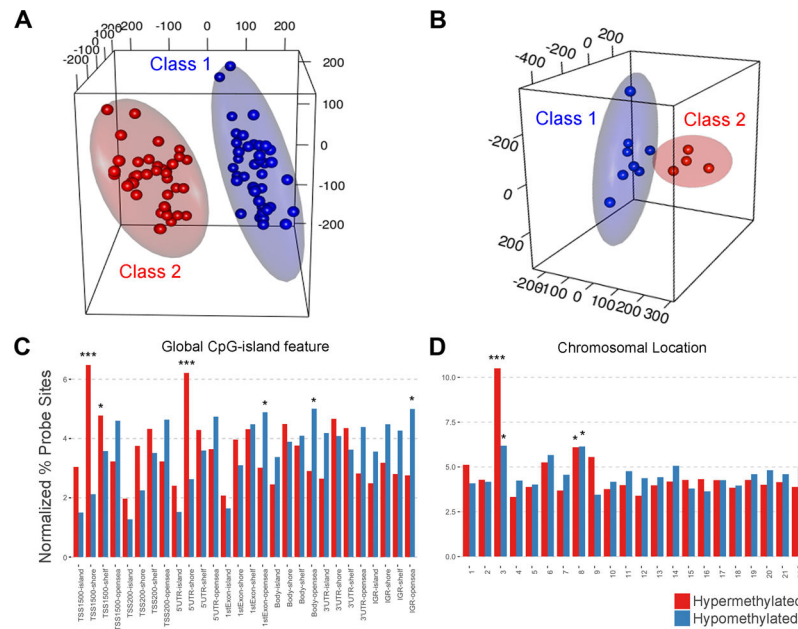


Figure 1. Global methylation analysis in primary uveal melanomas (UMs). (A) Unsupervised principal component analysis (PCA) based on methylation profiling showing differential clustering of Class 2 (red) and Class 1 (blue) UMs from the 80 TCGA cases. (B) Unsupervised PCA analysis on an independent dataset consisting of 12 additional cases that shows similar clustering based on methylation profiling. Red and blue ellipsoids represent 95% confidence intervals for each respective group. (C) Global CpG-island feature analysis of the normalized percent of hypermethylated (red) and hypomethylated (blue) probe sites in Class 2 UMs compared to Class 1 TCGA samples. (D) Chromosomal location analysis of the normalized percent of hypermethylated (red) and hypomethylated (blue) probe sites within the promoter region in Class 2 UMs compared to Class 1 TCGA samples. The promoter region was defined as starting at the transcription start site (TSS) and extending upstream 1500 base pairs. CpG-islands are defined as regions > 500 base pairs with > 55% GC content and an expected/observed CpG ratio of > 0.65. CpG shores are ~2Kb from islands and CpG shelves are ~4Kb from islands. * $p < 0.05$, ** $p < 0.01$, *** $p < 0.001$ with binomial testing.

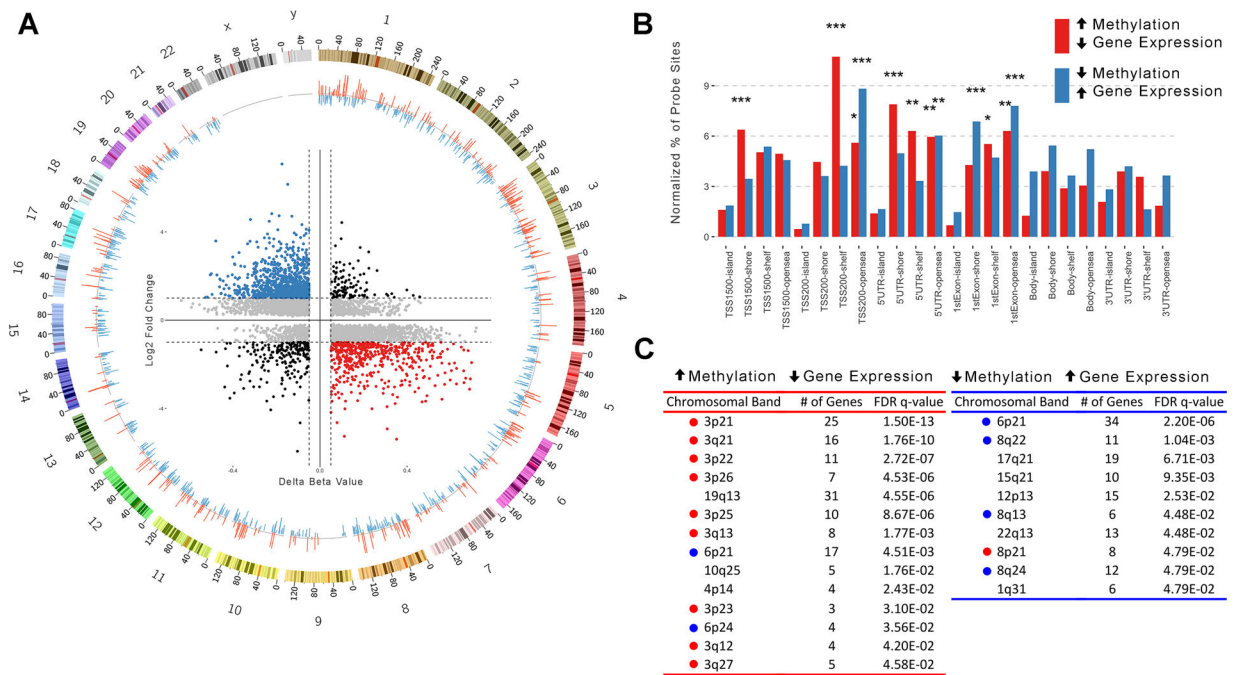


Figure 2.

Integration of DNA methylation with RNA expression data. (A) Inner quadrant graph demonstrates methylation of individual probe sites (x-axis, Class 2 Beta – Class 1 Beta) plotted against gene expression (y-axis, log₂ fold change Class 2/Class 1) in 80 TCGA samples. Red, hypermethylated/downregulated genes; blue, hypomethylated/upregulated genes; black, other genes. Outer Circos plot demonstrates hypermethylated/downregulated genes (red bars) and hypomethylated/upregulated genes (blue bars) that met filtering cutoffs (Delta Beta \pm 0.05 and log₂ fold change \pm 1) with respect to chromosomal location. (B) Global CpG-island feature analysis of the filtered hypermethylated/downregulated genes and hypomethylated/upregulated genes showing the normalized percent of hypermethylated (red) and hypomethylated (blue) probe sites. (C) Gene set enrichment analysis of chromosomal location for hypermethylated/downregulated genes (red lines) and hypomethylated/upregulated genes (blue lines) in Class 2 UMs compared to Class 1 UMs from the TCGA dataset. Copy number gains (blue circles) and losses (red circles) that commonly occur in UM on chromosomes 3, 6, and 8 are indicated next to the enriched methylated chromosomal regions. CpG-islands are defined as regions > 500 base pairs with > 55% GC content and an expected/observed CpG ratio of > 0.65. CpG shores are ~2Kb from islands and CpG shelves are ~4Kb from islands. *p < 0.05, **p < 0.01, ***p < 0.001 with binomial testing.

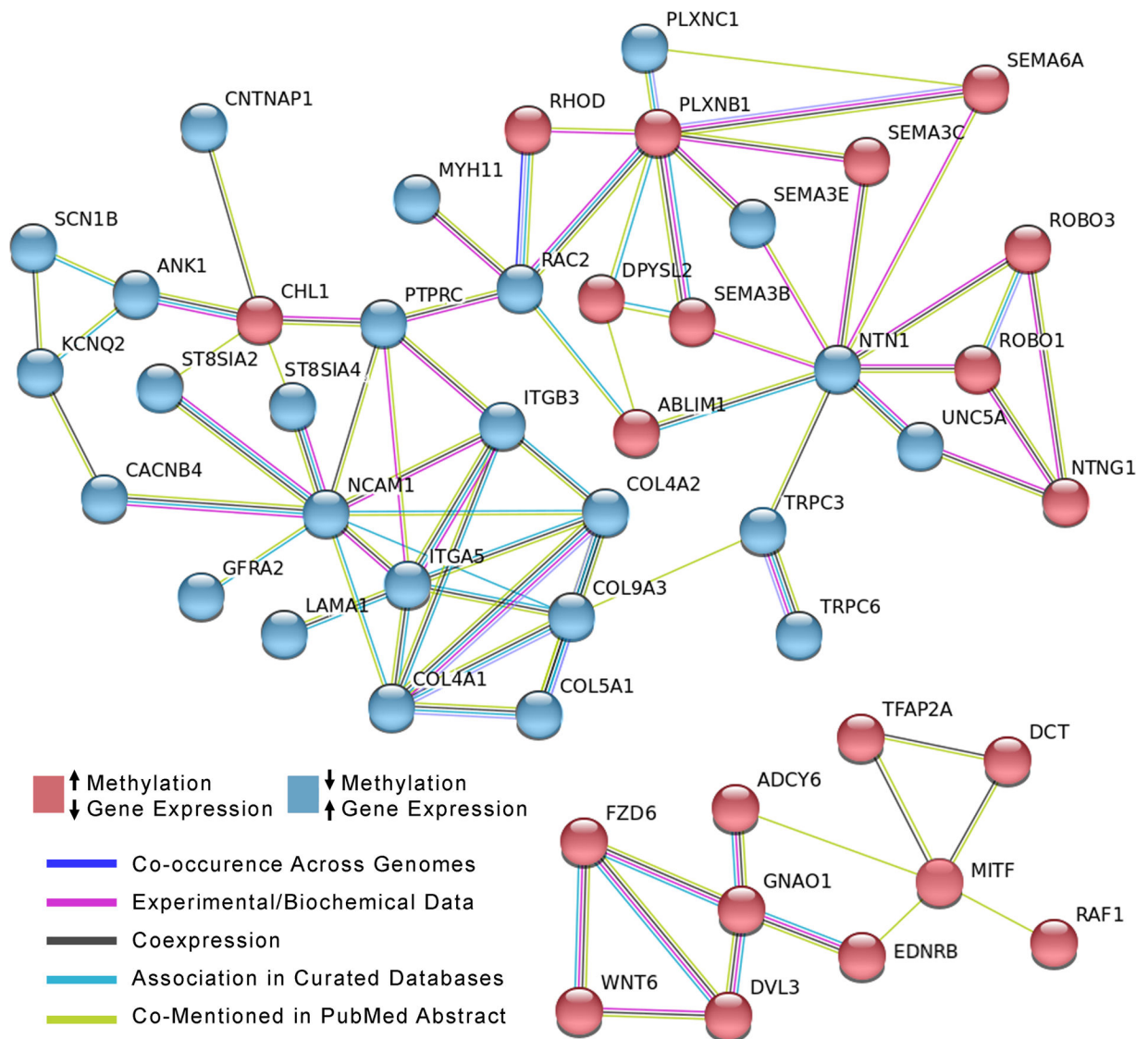


Figure 3. Epigenetic deregulation of axon guidance and melanogenesis pathways. Protein-protein interaction network of axon guidance (top) and melanogenesis (bottom) pathways identified using STRING, Gene Set Enrichment Analysis (GSEA), and the Molecular Signatures Database (MSigDB) for hypermethylated/downregulated (red) and hypomethylated/upregulated (blue) genes in Class 2 UMs compared to Class 1 UMs from the TCGA dataset. The source of evidence for each interaction is indicated by the legend.

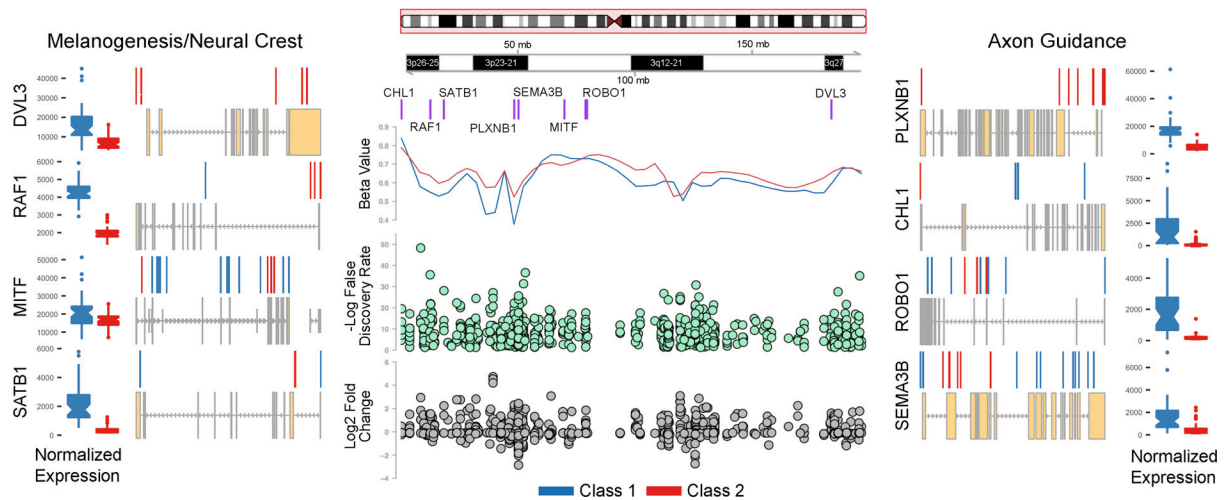


Figure 4.

Epigenetic silencing of key melanocyte-related developmental genes on chromosome 3 in Class 2 uveal melanoma. (Left) Melanogenesis and neural crest genes (*SATB1*, *MITF*, *RAF1*, *DVL3*) with box plots of normalized RNA read counts for all Class 1 UMs (blue) and Class 2 UMs (red) from the TCGA dataset with gene track plots of hypermethylated (red) and hypomethylated (blue) probe sites. (Middle, Top to Bottom) Ideogram of chromosome 3; Gene region with hypermethylated/downregulated loci (3p26–25, 3p23–21, 3q12–21, 3q27); Genomic location (purple bars) of hypermethylated/downregulated genes involved in axon guidance, neural crest, and melanogenesis; LOESS plot of DNA methylation (Beta Value) on chromosome 3 in Class 2 UMs (red line) and Class 1 UMs (blue line) from the TCGA dataset, including all probe sites associated with significantly hypermethylated/downregulated and hypomethylated/upregulated genes; Dot plot demonstrating significance ($-\log_{10}$ FDR) of differential methylation in Class 1 versus Class 2 UMs; Dot plot demonstrating fold change (\log_2 scale) in methylation in Class 1 versus Class 2 UMs. (Right) Axon guidance genes (*PLXN1*, *CHL1*, *ROBO1*, *SEMA3B*) with box plots of normalized RNA read counts for all Class 1 UMs (blue) and Class 2 UMs (red) from the TCGA dataset with gene track plots of hypermethylated (red) and hypomethylated (blue) probe sites. For box-and-whiskers plots, the central box represents the 25th to 75th percentiles, the middle of the notch represents the median, whiskers extend from the box hinges to 1.5 times the interquartile range (IQR), and outlier values that extend beyond the whiskers are indicated by dots. Notches within the central box extend $1.58 \cdot \text{IQR} / \sqrt{n}$, which gives a 95% confidence interval for comparing whether medians of box plots are significantly different.

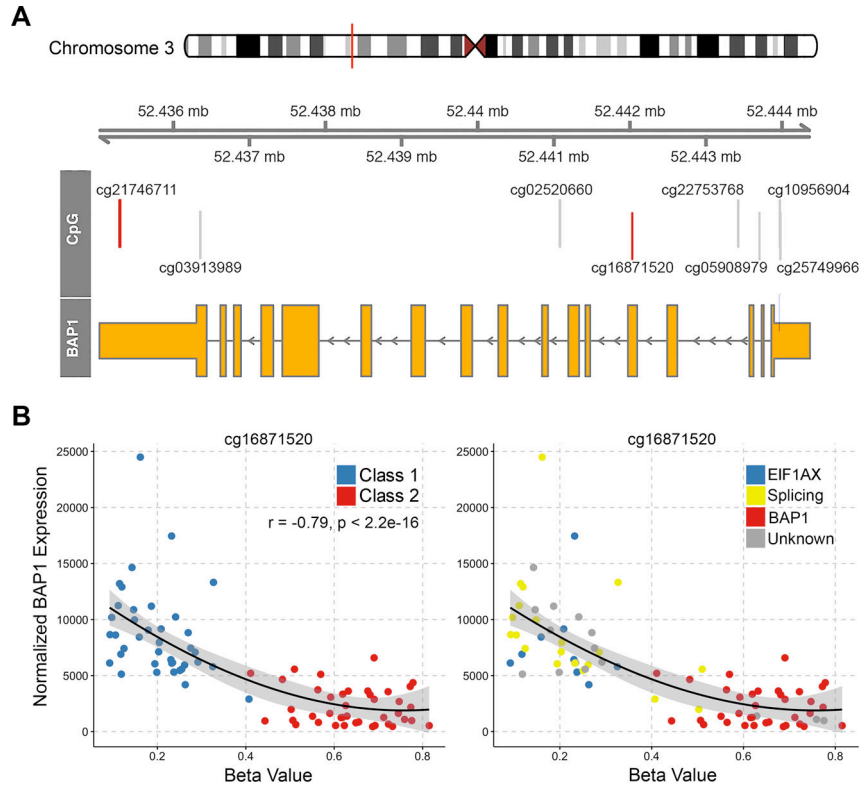


Figure 5. Association between *BAP1* methylation status, *BAP1* gene expression, molecular prognostic classification, and BSE mutation status. (A) Chromosome 3 ideogram with the *BAP1* locus indicated at chr3p21 (red bar), an expanded map of *BAP1* locus (chr3:52435020–52444121), with exons indicated by boxes, and direction of transcription indicated by arrows. Significantly methylated (red bars) and non-significantly methylated (grey bars) CpG probe sites within the *BAP1* locus are indicated. (B) Normalized *BAP1* gene expression plotted against methylation (Beta Value) of cg16871520, the most significantly hypermethylated probe site in Class 2 UMs relative to Class 1 UMs. LOESS linear regression line (black) is plotted along with the 95% confidence interval (grey). The r- and p-values were calculated using Spearman correlation coefficient. The left graph illustrates Class 1 versus Class 2 molecular prognostic classification status. The right graph highlights the BSE (*BAP1*, *SF3B1* and other splicing factors, and *EIF1AX*) mutation status.

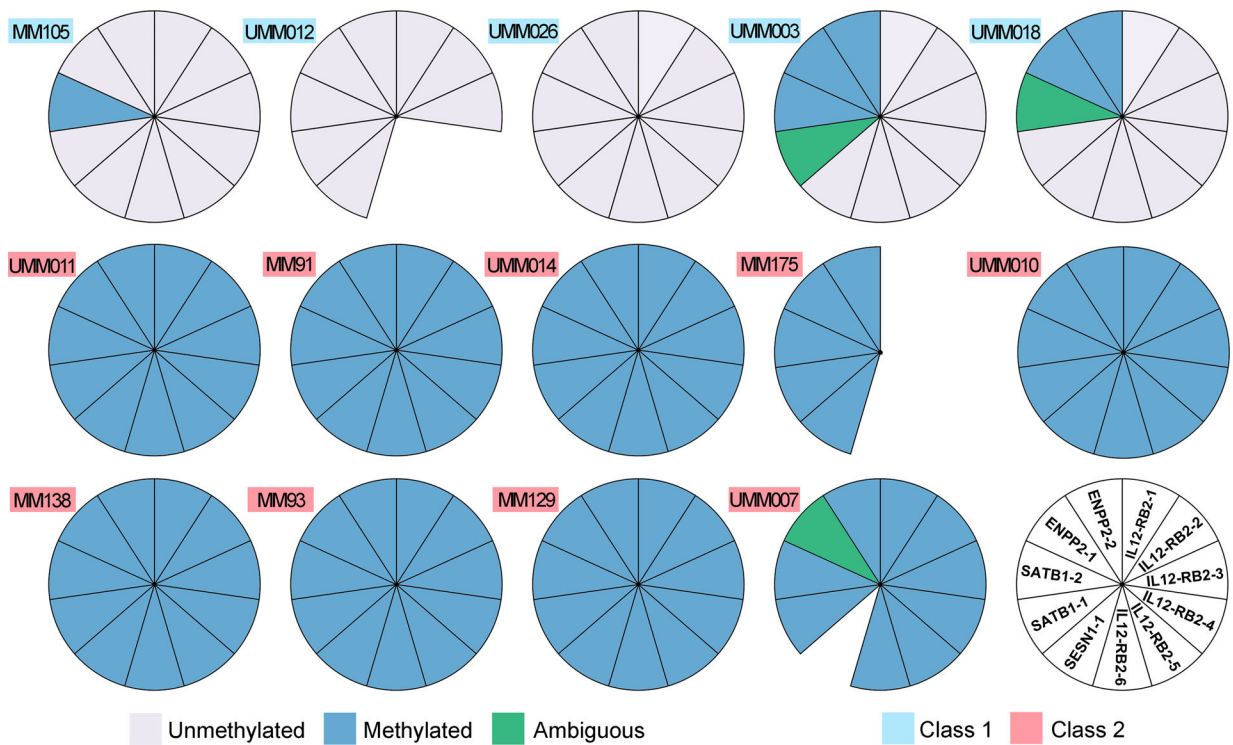


Figure 6. Orthogonal validation of highly differentially methylated CpG sites between Class 1 and Class 2 uveal melanomas. Fourteen UM samples that were previously unexamined for methylation were analyzed using the bisulfite conversion followed by Sanger sequencing for methylation of CpG sites within the *IL12RB2*, *SESN1*, *SATB1*, and *ENPP2* genes (see legend at lower right). Methylation calls are displayed in pie chart form. Grey, non-methylated; blue, methylated; green, ambiguous methylation. Masked Class 1 and Class 2 predictions based on methylation (blue and red boxes, respectively) corresponded to the UM gene expression profile in all cases. Absent pie pieces indicate technical failure.